Supporting Material

Probing the Structure of the Mechanosensitive Channel of Small Conductance in Lipid Bilayers with Pulsed Electron-Electron Double Resonance

Richard Ward,[†] Christos Pliotas,[†] Emma Branigan,[†] Christian Hacker,[‡] Akiko Rasmussen,[§] Gregor Hagelueken,[¶] Ian R. Booth,[§] Samantha Miller,[§] John Lucocq,[‡] James H. Naismith,[†*] and Olav Schiemann[¶,†,*]

[†]Centre for Biomolecular Sciences, University of St. Andrews, Scotland; [‡]School of Medicine, University of St. Andrews, Scotland; [§]Institute of Medical Sciences, University of Aberdeen, Scotland; and [¶]Institute of Physical and Theoretical Chemistry, University of Bonn, Germany.

[*]Correspondence: jhn@st-andrews.ac.uk or schiemann@pc.uni-bonn.de

Richard Ward, Christos Pliotas and Emma Branigan contributed equally to this work

FIGURE S1

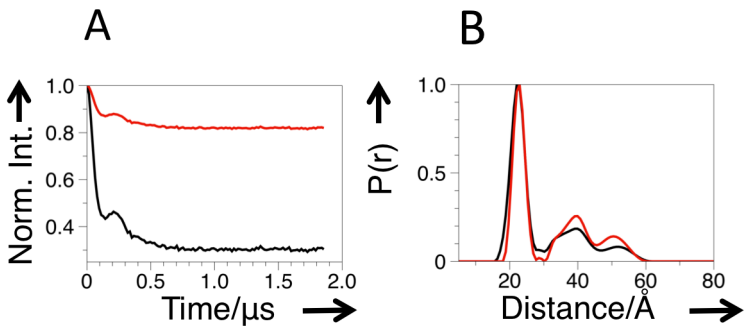

Supplemental Figure S1. A) Background corrected PELDOR data analysed without (black line) or with (red line) power scaling for a seven spin system. B) DeerAnalysis derived distance distribution (alpha=10, determined by L curve), without (black line) and with (red line) power scaling for a seven spin system.

As can be seen from supplemental figure S1 the effects of power scaling within DeerAnalysis2013 result in minor differences to the distance distribution compared with no power scaling. We observe a very slight narrowing of the 1-2 distance distribution width but with no change to the modal distance, which is what our conclusions are based upon. For the longer distances the intensities are slightly increased.

FIGURE S2

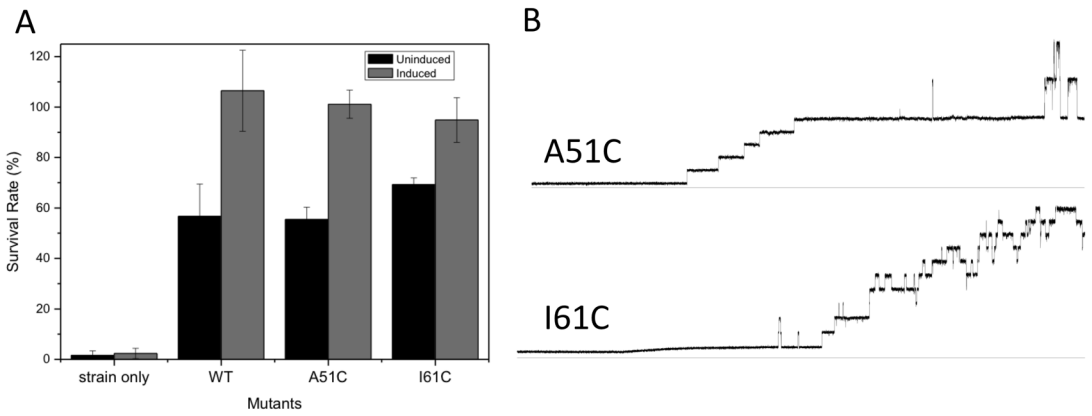

Supplemental Figure S2: A) Cell viability assay showing that cells containing mutant MscS A51 or I61C behave as wild type protein. B) Electrophysiology data for A51C and I61C showing that both proteins can gate (A51C PL:PS = 1.45 +/- 0.14, I61C = 1.79 +/- 0.06). However, while A51C behaves as wild type, I61C appears to show a slight gain-of-function phenotype, i.e. the channel is easier to open, but the open state is not as stable as wild type.

Figure S3

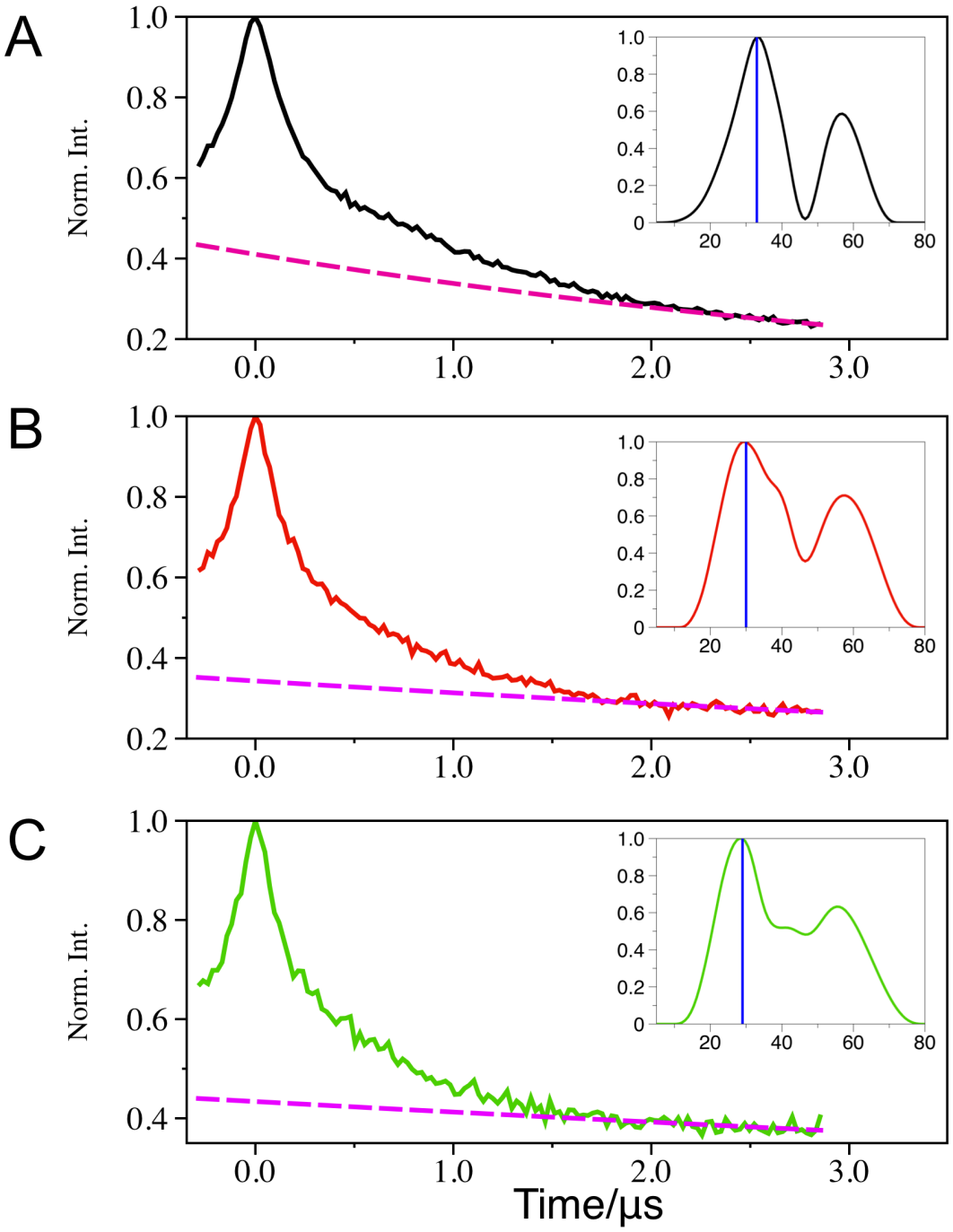

Supplemental Figure S3. MscS M47 PELDOR data. A), B) and C) show the raw data obtained for MscS M47R1 in DDM, bicelles and nanodiscs, respectively. Inset shows the distance distribution in angstrom obtained using Tikhonov regularisation in DeerAnalysis2013. We judge only A) to contain an oscillation and thus would use the 1-2 distance distribution for further discussion. That this is reasonable can also be seen from the narrower distance distribution for A compared with the other two.

Figure S4

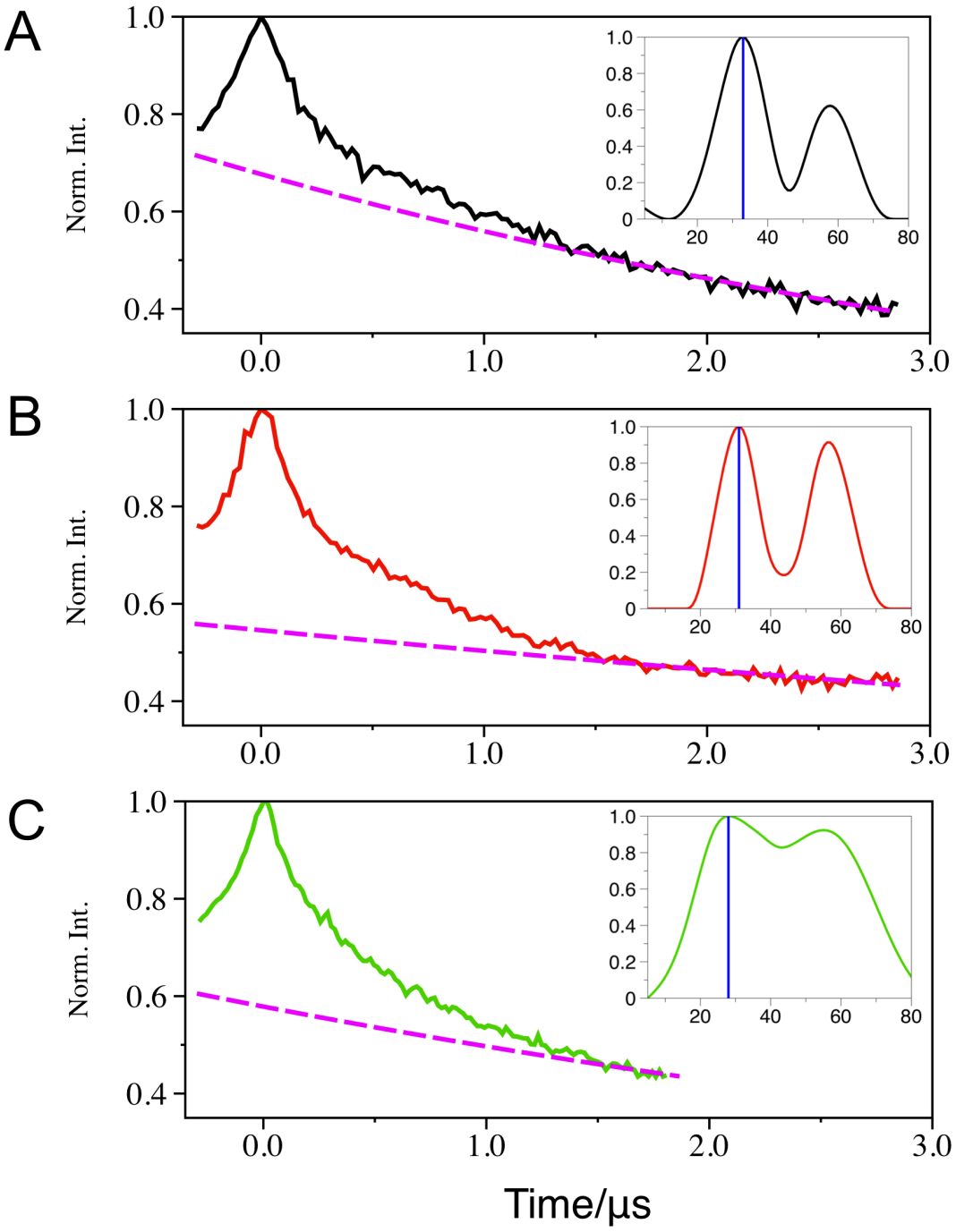

Supplemental Figure S4. MscS A51 PELDOR data. A), B) and C) show the raw data obtained for MscS A51R1 in DDM, bicelles and nanodiscs, respectively. Inset shows the distance distribution in angstrom obtained using Tikhonov regularisation in DeerAnalysis2013. We judge only B) to contain an oscillation and thus would use the 1-2 distance distribution for further discussion.

Figure S5

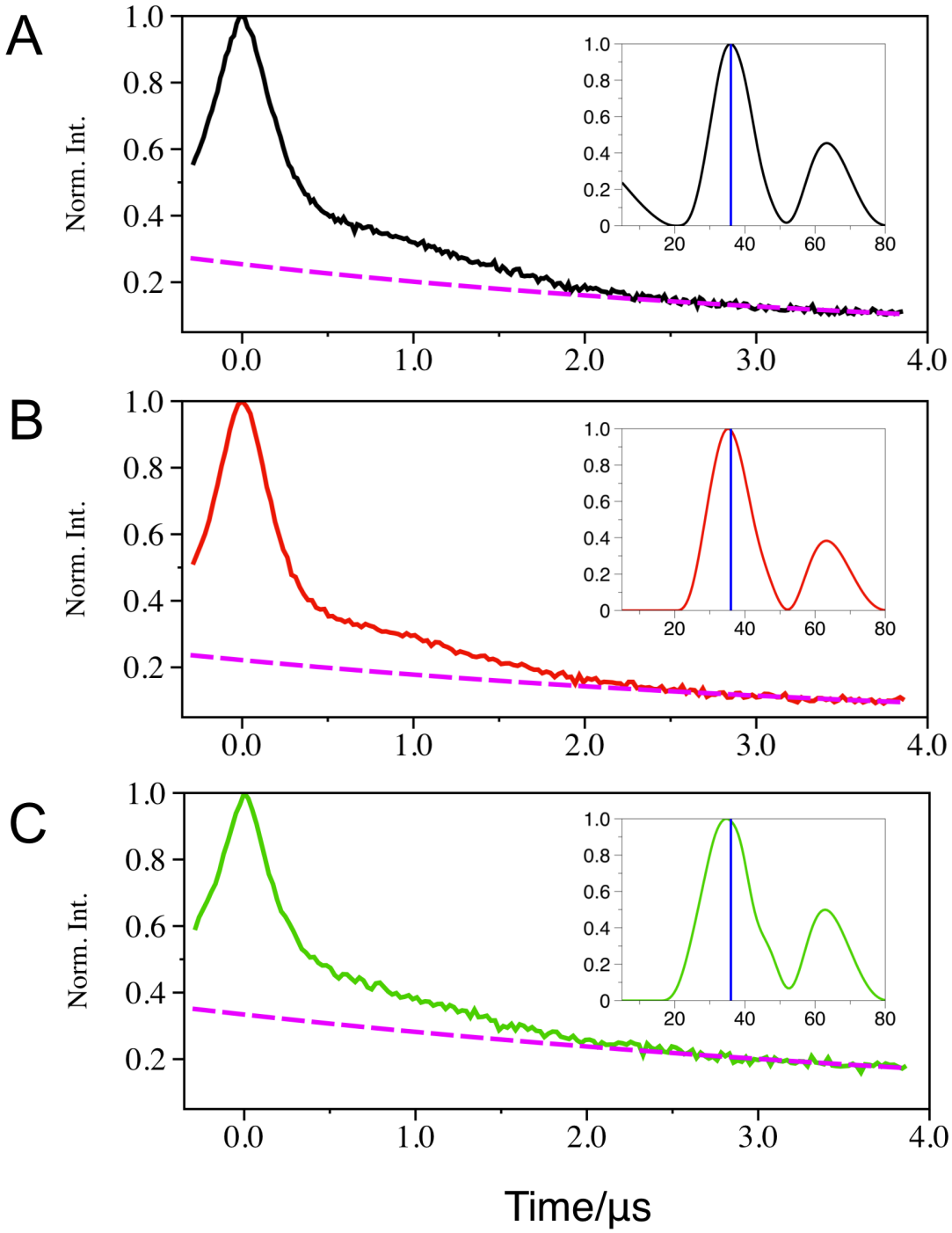

Supplemental Figure S5. MscS S58 PELDOR data. A), B) and C) show the raw data obtained for MscS S58R1 in DDM, bicelles and nanodiscs, respectively. Inset shows the distance distribution in angstrom obtained using Tikhonov regularisation in DeerAnalysis2013. We judge A-C) to contain an oscillation and thus would use the 1-2 distance distribution for further discussion.

Figure S6

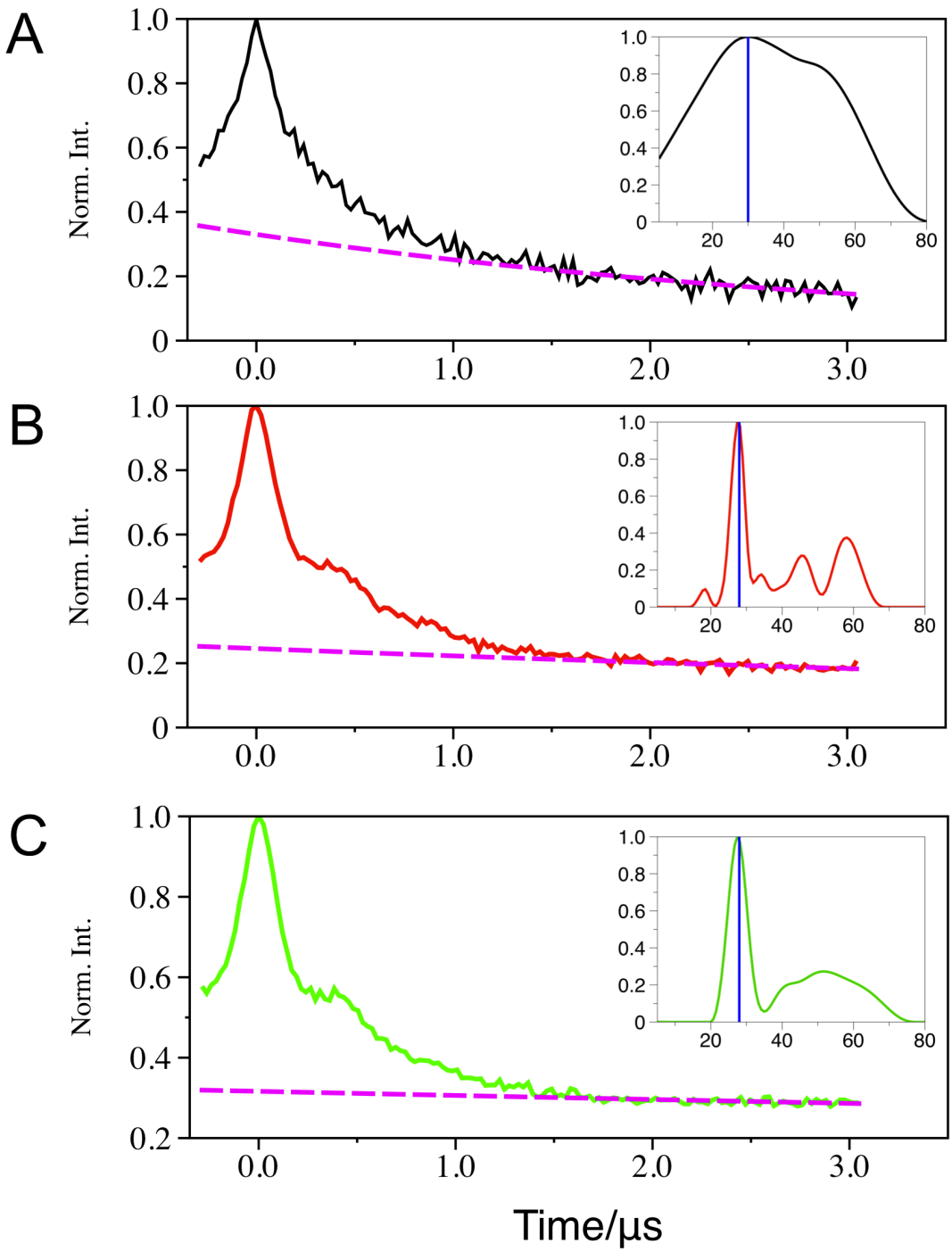

Supplemental Figure S6. MscS I61 PELDOR data. A), B) and C) show the raw data obtained for MscS I61R1 in DDM, bicelles and nanodiscs, respectively. Inset shows the distance distribution in angstrom obtained using Tikhonov regularisation in DeerAnalysis2013. We judge B) and C) to contain an oscillation and thus would use the 1-2 distance distribution for further discussion.

Figure S7

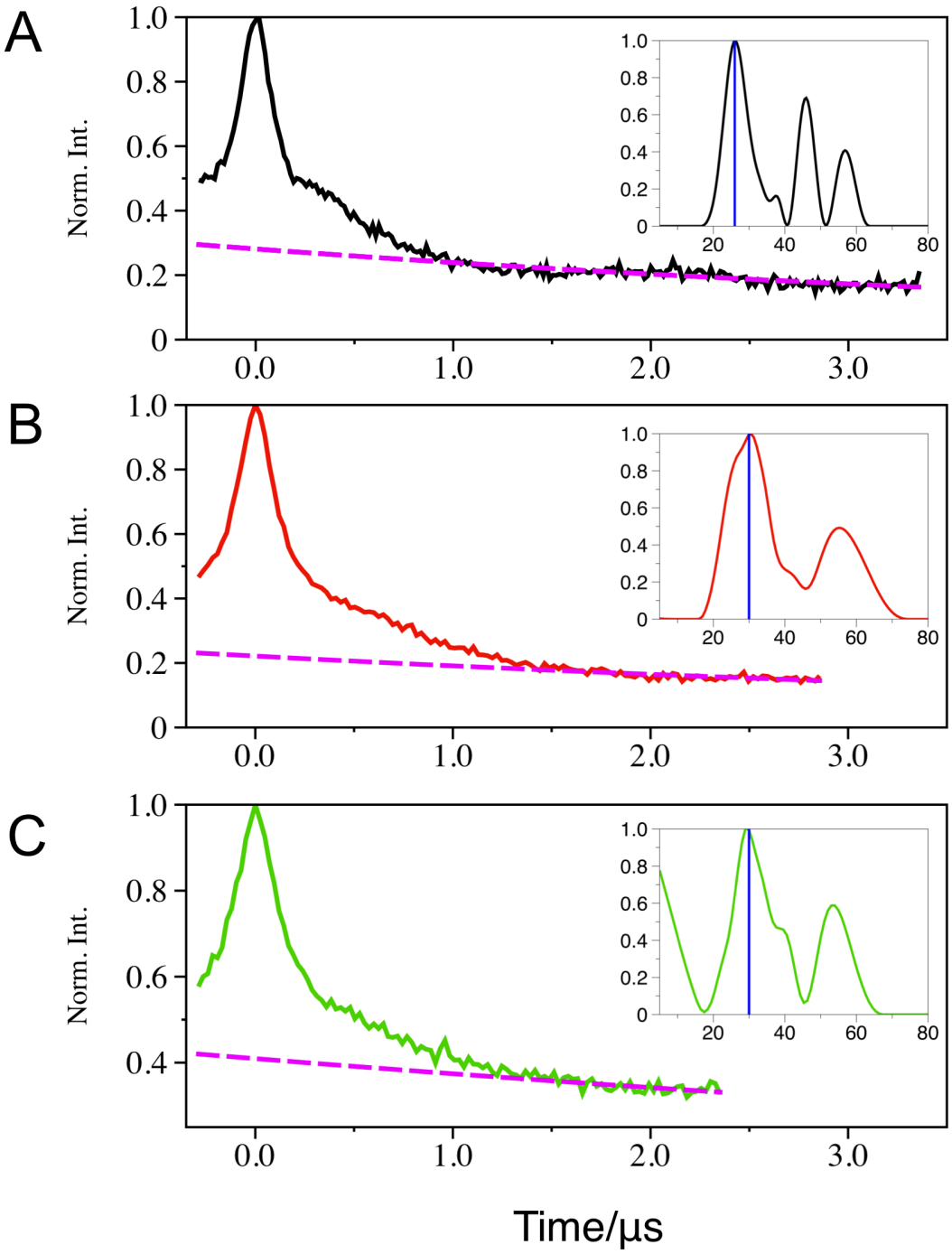

Supplemental Figure S7. MscS D67 PELDOR data. A), B) and C) show the raw data obtained for MscS D67R1 in DDM, bicelles and nanodiscs, respectively. Inset shows the distance distribution in angstrom obtained using Tikhonov regularisation in DeerAnalysis2013. We judge A-C) to contain an oscillation and thus would use the 1-2 distance distribution for further discussion.

Figure S8

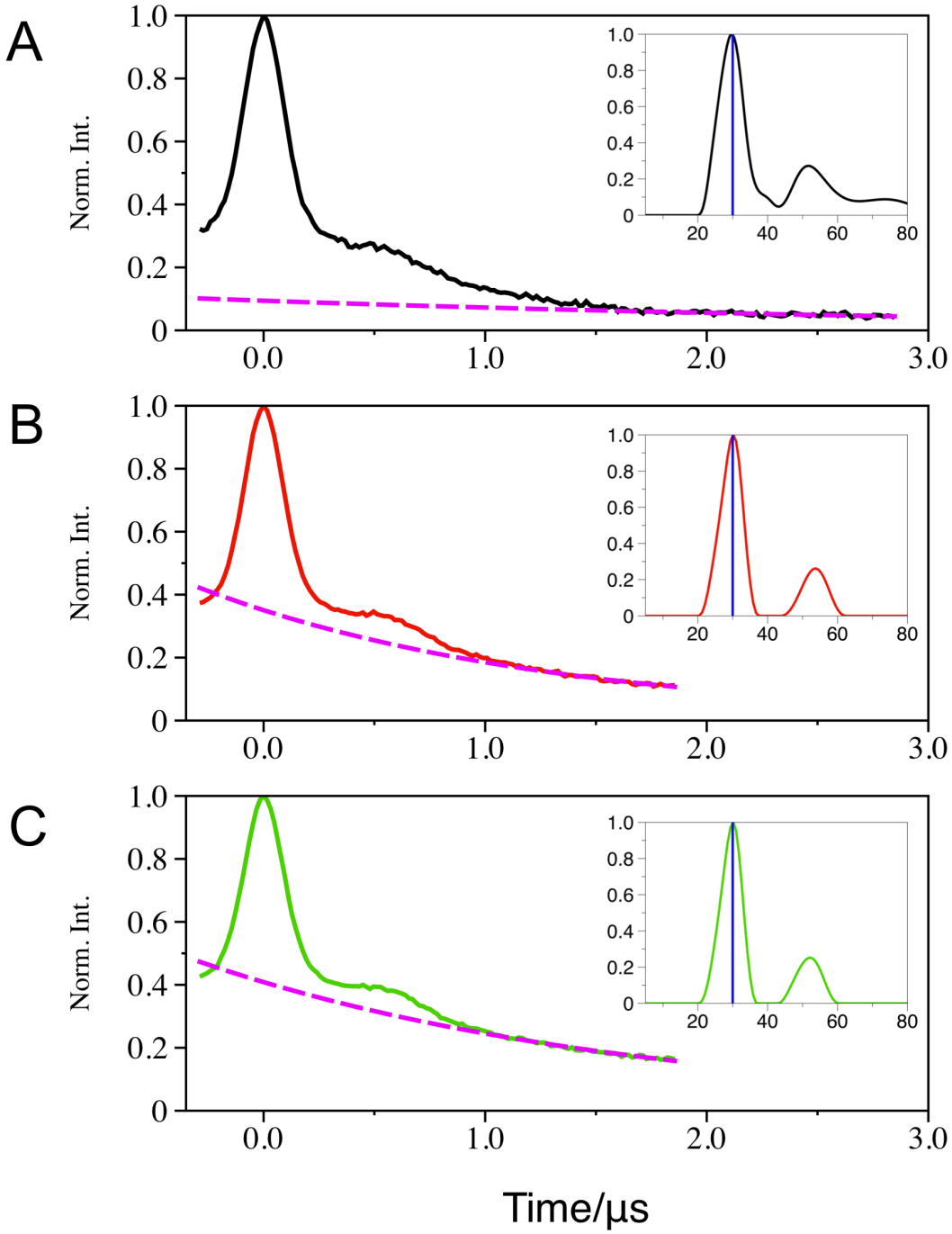

Supplemental Figure S8. MscS S147 PELDOR data. A), B) and C) show the raw data obtained for MscS S147R1 in DDM, bicelles and nanodiscs, respectively. Inset shows the distance distribution in angstrom obtained using Tikhonov regularisation in DeerAnalysis2013. We judge A-C) to contain an oscillation and thus would use the 1-2 distance distribution for further discussion.

Figure S9

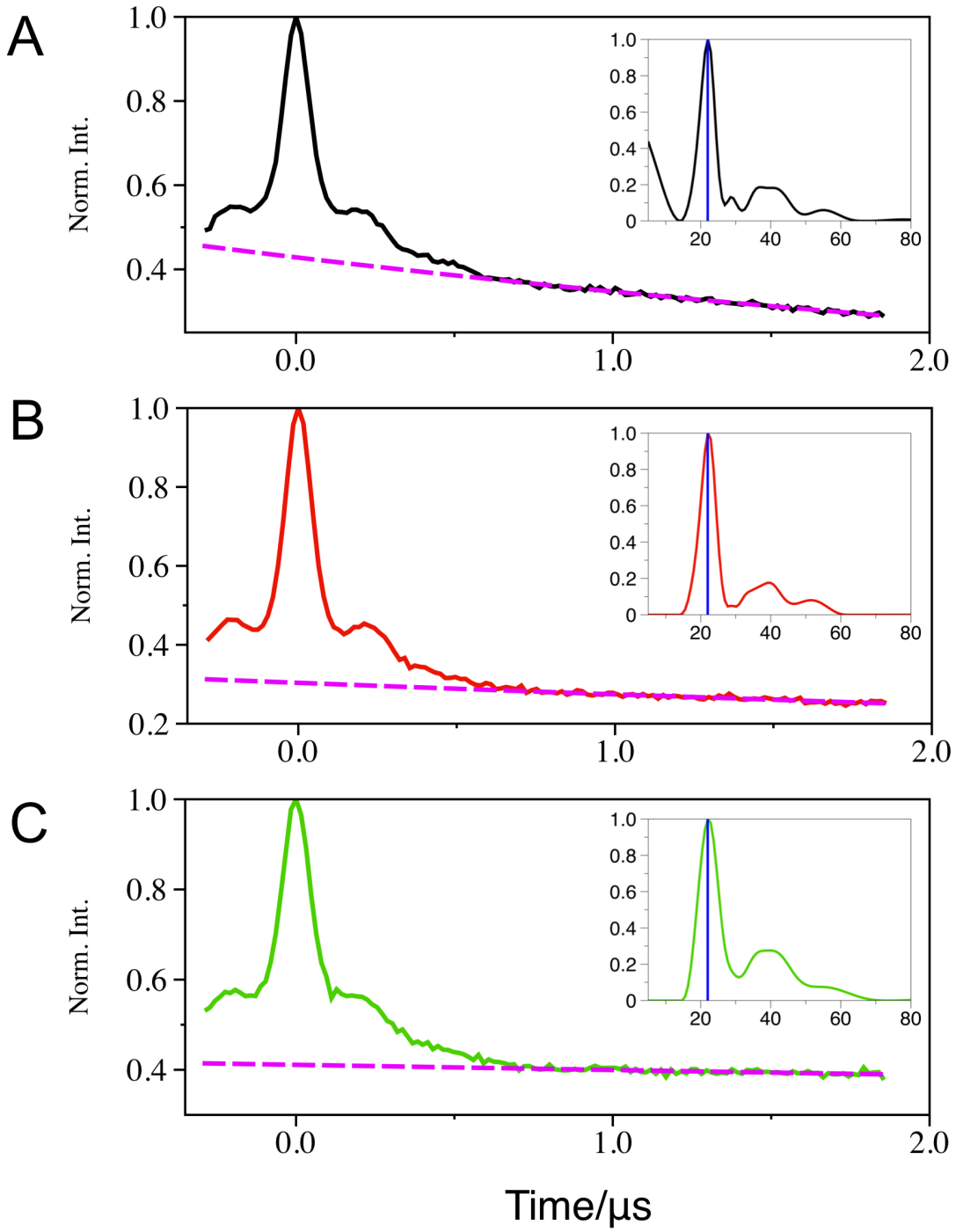

Supplemental Figure S9. MscS S196 PELDOR data. A), B) and C) show the raw data obtained for MscS S196R1 in DDM, bicelles and nanodiscs, respectively. Inset shows the distance distribution in angstrom obtained using Tikhonov regularisation in DeerAnalysis2013. We judge A-C) to contain an oscillation and thus would use the 1-2 distance distribution for further discussion.

FIGURE S10

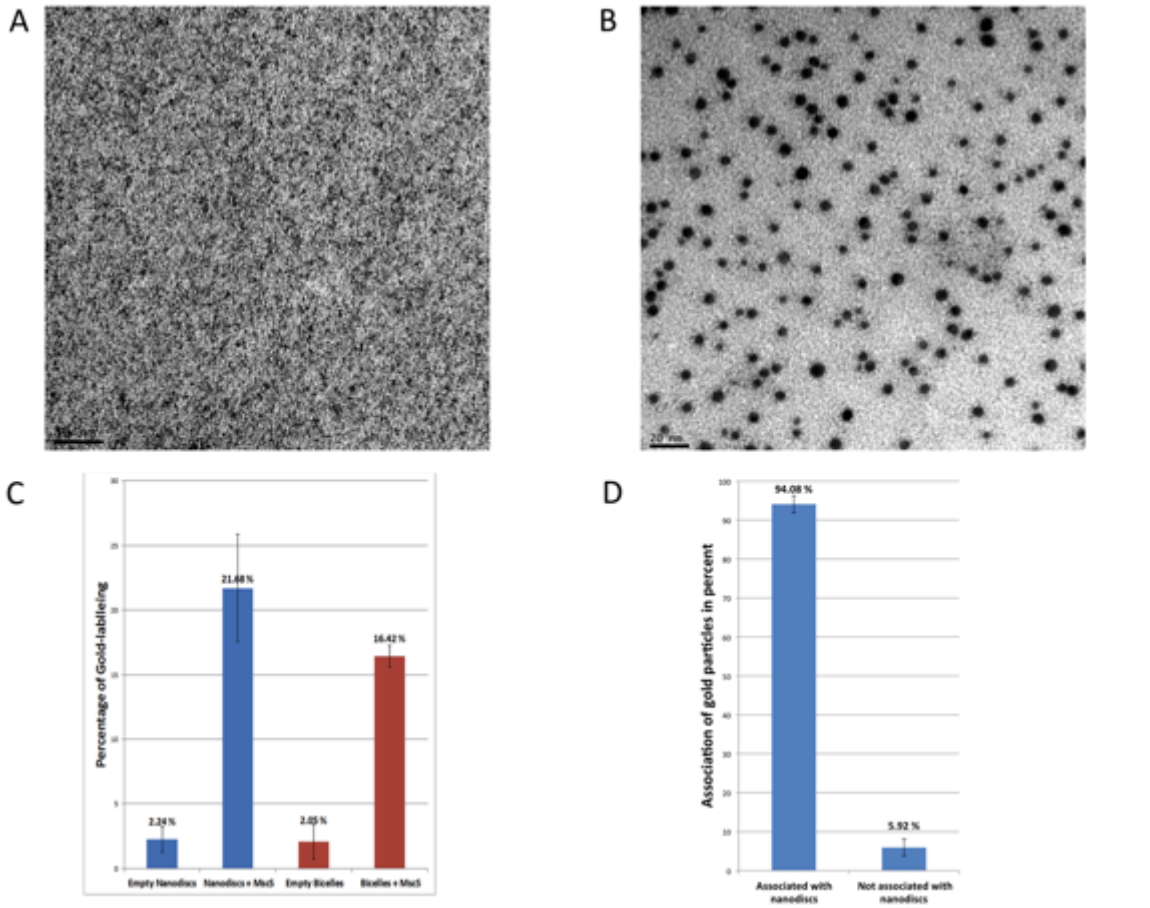

Supplemental Figure S10: NTA-nanogold labeled A) gel filtration buffer containing 0.05% DDM, 50 mM Na-phosphate pH 7.5 and 300 mM NaCl (i.e. no MscS is present), B) MscS D67R1 in identical buffer conditions (i.e. free protein in detergent). C) Mean percentages of positively nickel-NTA gold-labeled nanostructures from three independent experiments. Nanostructures were sampled and quantified systematic uniform random using the forbidden line unbiased counting rule (see Materials and Methods) and gold counts made. Error bars indicate the standard error of the mean. D) Mean percentage of nickel-NTA nanogold either associated (94%) with nanodiscs or not (6%).

From supplemental figure S10 we can see by comparing (A) and (B) that MscS in detergent is readily labeled with the NTA-nanogold reagent. Therefore if there was “free” MscS present in the nanodisc or bicelle reconstitutions we would expect to see it clearly. However, in Figure 2 the nanogold is predominantly associated (94%) with either the nanodiscs or the bicelles.

FIGURE S11

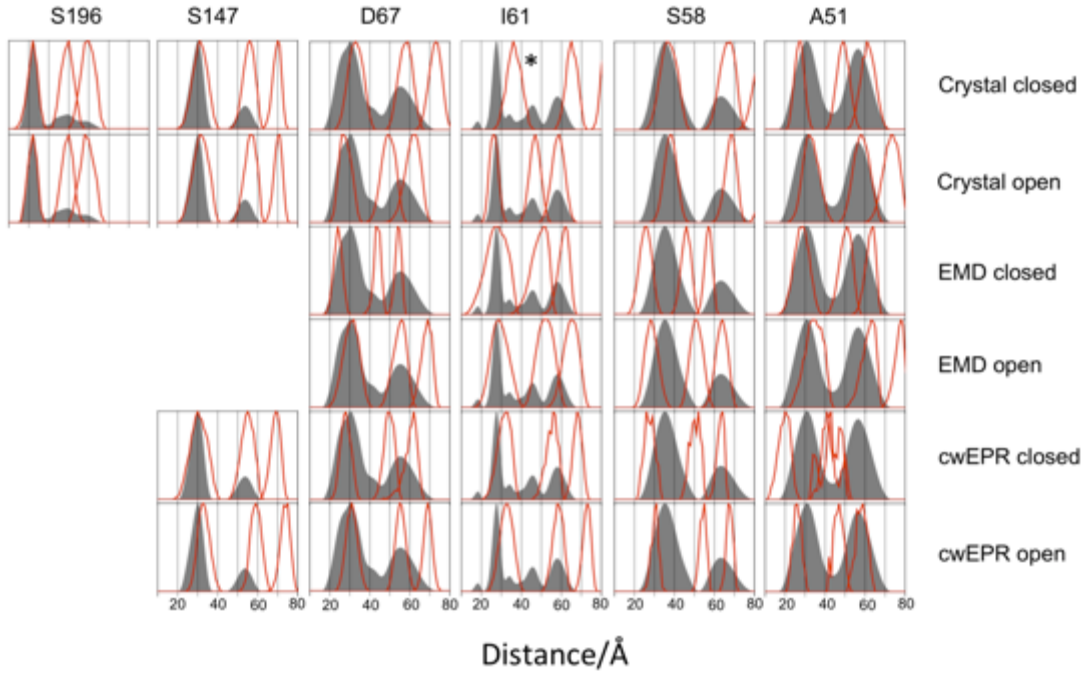

Supplemental Figure S11. Comparison of mtsslwizard derived and experimentally determined distance distributions for each model at each labelling position. PELDOR derived distance distributions shown as grey shaded area. Mttslwizard derived distance distributions shown as red lines. * I61 sits on a loop that is poorly defined in the 2oau structure and thus the distance distribution is questionable for this position, see supplemental figure S5.

FIGURE S12

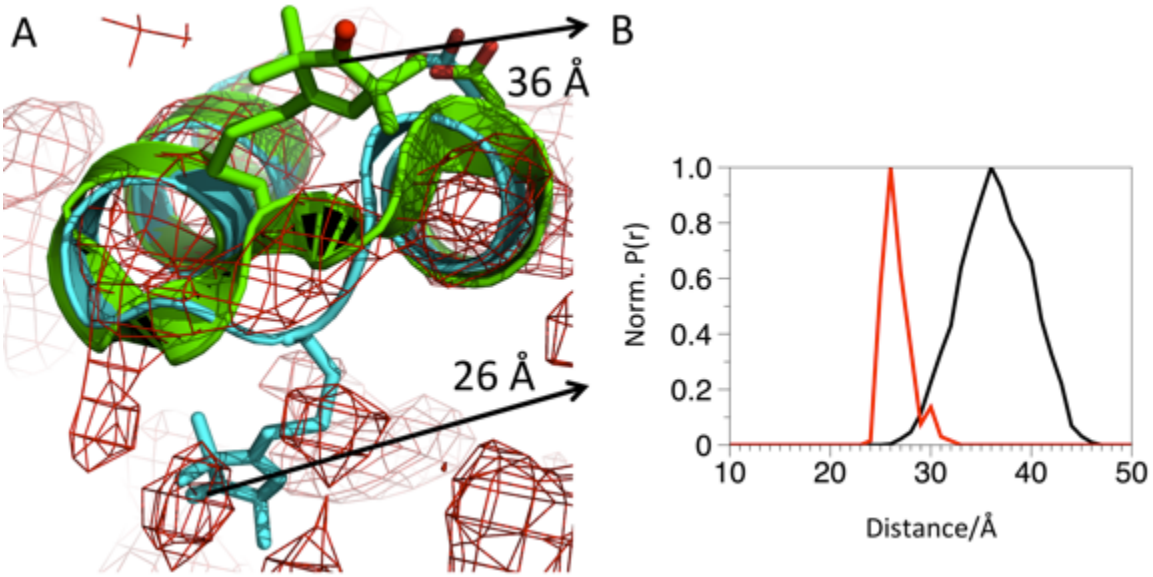

Supplemental Figure S12: A) Overlay of cartoon representation of closed (2oau) and open (2vv5) crystal structures, with the electron density mesh for 2oau. The structures are colored green and blue for the closed and open structures, respectively. The electron density mesh (red) is set to the 1 sigma level. The spin labeled residue I61 and the non-spin labeled D67 are shown as sticks for both structures. As can be seen, either the closed or open loops could be fitted into the electron density for this region, thus the exact position of I61 in the closed structure is not definite. This alignment of the TM1 and 2 helices results in most of the other side chains being in a similar orientation, the D67 side chain is shown as an example of this. B) Comparison of distance distributions obtained, using mtsslWizard, for I61 using the original 2oau structure (black line) or the hybrid structure of 2oau, partly shown in A, with the loop region from the higher resolution 2vv5 structure (red line).

FIGURE S13

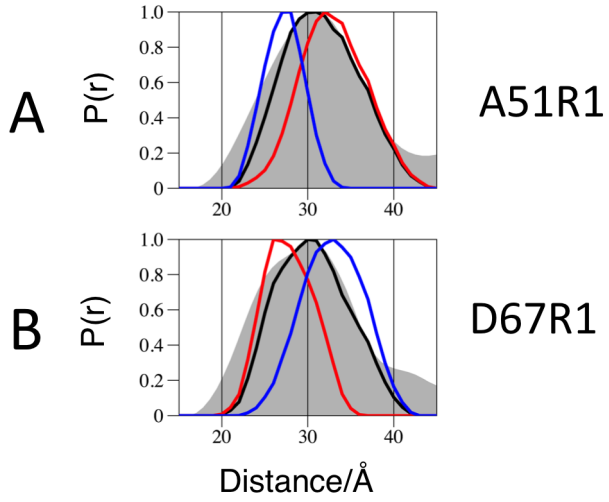

Supplemental Figure S13: Comparison of experimental 1-2 distance data (grey shaded area) with particular ratios of the Mtsslwizard derived 1-2 distance distributions for 2oau and 2vv5 (black line). A) EPR data for A51R1 compared with a 1:2 ratio of 2oau(closed):2vv5(open). B) EPR data for D67R1 compared with a 1:1 ratio of 2oau(closed):2vv5(open). The 100% 2oau or 2vv5 1-2 distance distributions obtained by Mtsslwizard are shown in blue or red, respectively.